

# A hyperlens-based device for nanoscale focusing of light

Jiangnan Zhao (赵江南), Guoxing Zheng (郑国兴)\*, Song Li (李松), Hui Zhou (周辉),  
Yue Ma (马跃), Ruiying Zhang (张瑞瑛), Yan Shi (石岩), and Ping'an He (何平安)

School of Electronics Information, Wuhan University, Wuhan 430072, China

\*Corresponding author: gxzheng@whu.edu.cn

Received August 18, 2011; accepted October 8, 2011; posted online November 25, 2011

To resolve the problem of missed evanescent waves in a beam focusing system, a hyperlens-based beam focusing device is proposed in this letter. This device can convert the evanescent waves into propagating waves, and then a super-resolution spot is formed at the center of the hyperlens. The working principle of the device is presented, and the way in which the material and structural parameters of the hyperlens affect the resolution and transmission is analyzed in detail. A multibeam focusing device is optimally designed, and the simulated results verify that a nanoscale spot with a diameter of 15.6 nm (corresponding to  $\lambda_0/24$ , where  $\lambda_0$  is the working wavelength in vacuum) is achieved, which is far less than the diffraction limited resolution with a value of 625 nm ( $1.7\lambda_0$ ). The device is expected to find numerous applications in optical data storage and nano-photolithography, among others.

OCIS codes: 230.0230, 160.3918, 220.3630, 350.4238.

doi: 10.3788/COL201210.042302.

In an optical data storage and nano-lithography area, an ultra-small beam spot is required for information recording. With the phase transformation of an ideal positive lens, an input plane wave can be converted into a converging spherical wave and then eventually focused into a point at the focal plane. However, limited by diffraction, the ideal focusing point is through an Airy pattern. This can be explained by the fact that when the beam is focused toward the focal plane, the conservation of the angular momentum forces the tangential wave vector  $k_\theta$  to increase toward the center, however, light with  $k_\theta > k_0$  corresponds to the evanescent wave that cannot reach the focal plane, where  $k_0$  is the wavenumber in vacuum. According to the equation  $\Delta x \Delta k \approx 2\pi^{[1]}$ , where  $\Delta x$  is the beam size and  $\Delta k$  is the bandwidth of the angular spectrum, the maximum  $\Delta k$  that could be delivered is determined by the maximum transverse wavenumber  $k_0 \times \text{NA}$  ( $\Delta k = k_0 \times \text{NA}$  and NA is the numerical aperture of the focusing lens) and the minimum beam size  $\Delta x$  is  $\lambda_0/\text{NA}$ , which corresponds to the diffraction limit. To further reduce the beam size, we should find materials that allow waves with transverse wavenumber exceeding  $k_0 \times \text{NA}$  to propagate in it with a propagating wave mode, instead of an evanescent wave mode. Conventional isotropic materials such as optical glasses do not show such characteristics, whereas artificial materials such as metamaterials<sup>[2]</sup> hold such potential. By optimization design<sup>[3–5]</sup>, metamaterials can achieve the desired effective dielectric permittivity  $\varepsilon$  and magnetic permeability  $\mu$  and have been theoretically shown to support propagating waves with very large wavenumbers. Lens fabricated by metamaterials, such as near-field planar superlens<sup>[6,7]</sup>, far-field superlens<sup>[8]</sup>, and hyperlens<sup>[9–12]</sup>, can support the propagation of evanescent waves and thus are capable of imaging an ultra-small object far below the diffraction limit. In this letter, we concentrate on another application and report on how a hyperlens-based device can work for super-resolution beam focusing.

The hyperlens consists of alternating metallic and dielectric layers in a cylinder- or sphere-shape. According

to the effective medium theory<sup>[4]</sup>, a cylinder-shape hyperlens is equivalent to a structured metamaterial with effective positive tangential dielectric permittivity  $\varepsilon_\theta$  and negative radial dielectric permittivity  $\varepsilon_r$ . Meeting the hyperbolic dispersion relation  $k_r^2/\varepsilon_\theta - k_\theta^2/|\varepsilon_r| = k_0^2$ <sup>[9]</sup> in cylindrical coordinates, hyperlens with its ring structure allows far-field propagation for the propagating waves (not evanescent waves) with the tangential wave vector  $k_\theta$  larger than  $k_0$ . The working principle of a hyperlens-based beam focusing device is illustrated in Fig. 1. In Fig. 1(a), the dimension of the converging wave will no longer be reduced starting at the focal plane of the focusing lens marked with  $B$  for the diffraction limit. However, if a half-spherical hyperlens is inserted between plane  $A$  and plane  $B$  with its bottom planar surface coinciding with plane  $A$  (the ideal focal plane), the converging wave will be re-focused, and waves with tangential wave vectors  $k_\theta$  larger than  $k_0$  will undergo propagating modes in the hyperlens and continue focusing until they eventually reach the ideal focal plane  $A$ , leading to a super-resolution focusing spot.

The material and structural parameters of the hyperlens should be optimized to obtain a high resolution (or beam spot size) and system transmission. The resolution is related to the wavenumber. According to the above analysis, when the beam focuses into the core, the largest transverse wavenumber that could be delivered is  $(R_2/R_1)k_0 \times \text{NA}$ , where  $R_1$  and  $R_2$  are the radii of the outmost and innermost layers of the hyperlens, respectively, and the corresponding resolution Res can be expressed as follows:

$$\text{Res} = \frac{\lambda_0}{2\text{NA}(R_2/R_1)}. \quad (1)$$

From Eq. (1), we can see that the resolution improves along with the increasing of  $R_2/R_1$  and that the ideal spot can be obtained when  $R_1$  is approximate to zero (corresponding to a half-spherical hyperlens, as seen in Fig. 1(b)).

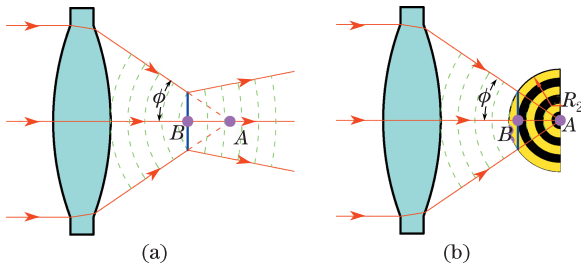


Fig. 1. Working principle of the super-resolution focusing with (a) a single focusing lens and (b) a hybrid beam focusing device with focusing lens and hyperlens.

The outmost layer intersects with plane B, as illustrated in Fig. 1(b), and its radius  $R_2$  satisfies

$$R_2 = \frac{\lambda_0}{4 \tan \phi \sin \phi}, \quad (2)$$

where  $\phi$  is the half aperture angle of the ideal beam focusing system.

In a hyperlens, we assume that all incident rays propagate toward the core to produce a small focusing spot, however, the actual incident beam consists of complex waves and is divergent, which leads to beam deviation and spot spreading at the focal plane. The beam deviation can be determined by the intersection angle  $\alpha$  between the ray vector (Poynting vector  $\mathbf{S}$ ) and the radial wave vector  $k_r$  inside the hyperlens. By optimizing the material parameter, the angle  $\alpha$  can reduce to a small value. In a hyperlens, the angle  $\alpha$  increases with  $k_\theta$  and reaches its maximum at infinity, as shown in Fig. 2(a). The maximum angle  $\alpha_c$  is determined by the angle between the asymptotes of the hyperbola<sup>[11]</sup>.

$$\tan \alpha_c = \sqrt{\frac{\varepsilon_\theta}{|\varepsilon_r|}} = \sqrt{\frac{[p\varepsilon_m + (1-p)\varepsilon_d][(1-p)\varepsilon_m + p\varepsilon_d]}{-\varepsilon_m\varepsilon_d}}, \quad (3)$$

where  $p$  denotes the filling ratio of the metal, and  $\varepsilon_m$  and  $\varepsilon_d$  denote the dielectric permittivity of the metal and the dielectric layers, respectively. We plot  $\alpha_c$  versus  $p$  curves with two typical material combinations, and the results are shown in Fig. 2(b). As can be seen from the figure, the curves reach a peak value when  $p$  is 0.5 and different material combinations lead to different maximum angles  $\alpha_c$  for different operation wavelengths. Therefore, the material combination and the filling ratio  $p$  should be optimized to obtain a high resolution.

Transmission is another important characteristic of the hyperlens-based device. The loss arising in the device comes from the intrinsic loss of the metal<sup>[13,14]</sup>. Apparently, a thinner metal film leads to a lower loss, however, good-quality ultra-thin metal films are difficult to achieve and they have a relatively large imaginary part  $\text{Im}[\varepsilon_m]$  and the dielectric permittivity  $\varepsilon_m$  will not remain constant as it becomes a function of layer thickness<sup>[14]</sup>. Furthermore, the hyperlens with alternating layers of metal and dielectric differ with the superlens, which only has a single metal layer. Beams propagating in a hyperlens will undergo multibeam interference, field enhancement, and metal loss. Therefore, it is difficult to deduce an exact expression to describe the system transmission. However, some numerical algorithms such as the

transfer-matrix method<sup>[15,16]</sup> can be used to evaluate system transmission. The system transmission coefficient versus metal layer thickness is shown in Fig. 3, where the optimized thickness for the maximum transmission is about 56.5 nm for some concrete parameters of hyperlens. The thickness of the silver is chosen as 56.5 nm in the following numerical simulations.

To verify the ability of super-resolution focusing, we propose a hyperlens-based beam focusing system, as shown in Fig. 4. In a beam focusing application, the resolution and the transmission are both important. To compensate the metal loss and then improve the intensity of focusing spots, multibeam focusing lens are employed, as shown in Fig. 4(a). For example, a three-beam focusing device is designed, and Multiphysics 3.5 (COMSOL) is used to simulate the performances of the proposed hyperlens-based beam focusing device. The simulation results of the power flow traveling through three focusing lens and the hyperlens in the transverse-magnetic (TM) mode are shown in Fig. 4(b). In the simulations, the working wavelength is 375 nm and the main parameters of the focusing lens are as follows: focal length of 2  $\mu\text{m}$ , numerical aperture of 0.3, and lens material of silica. For the hyperlens in Fig. 4(b), the outmost radius  $R_2$  is 1.017  $\mu\text{m}$ , and the layer thickness is 56.5 nm with alternating  $\text{Al}_2\text{O}_3$  ( $\varepsilon_d=3.21$ ) and Ag ( $\varepsilon_m=-3.12+0.21i$ ). As

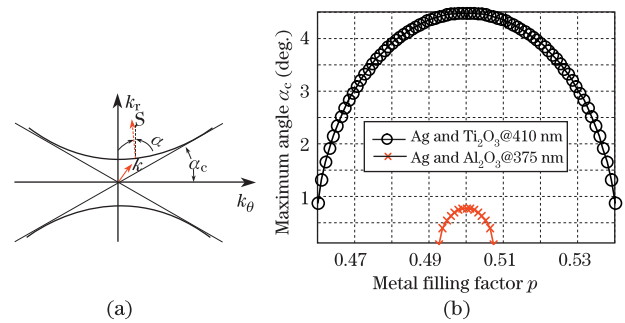


Fig. 2. (a) Hyperbolic dispersion relation for a hyperlens and (b) schematic of the maximum angle  $\alpha_c$  versus the metal filling factor  $p$ . For the curve marked with cross dots, the dielectric material is aluminum oxide with  $\varepsilon_d=3.21$ , the metal is silver with  $\varepsilon_m=-3.12 + 0.21i$ <sup>[13]</sup>, and the working wavelength is 375 nm. In another curve marked with circle dots, the dielectric material is titanium oxide with  $\varepsilon_d=5.83$ , the metal is silver with  $\varepsilon_m=-4.99+0.22i$ <sup>[13]</sup>, and the working wavelength is 410 nm.

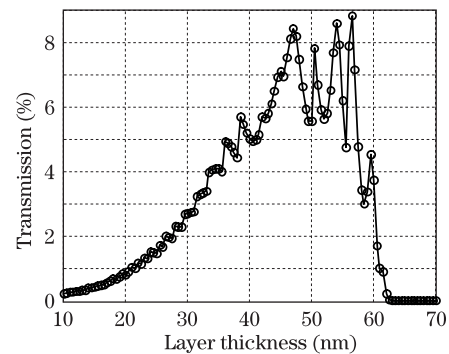


Fig. 3. Curve for the transmission coefficient versus metal thickness. In the simulation, light is in normal incidence and the simulation data are with a total layer thickness of the hyperlens of 1  $\mu\text{m}$ ,  $\varepsilon_m=-3.12+0.21i$ , and  $\varepsilon_d=3.21$ .

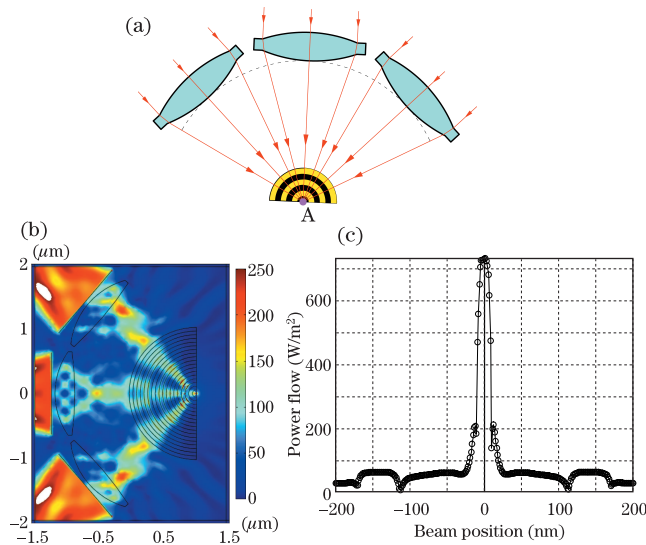


Fig. 4. (a) Schematic of a multibeam super-resolution focusing device, (b) the norm of the power flow distributions in the simulation domain; and (c) the power flow distributions in the cross-section direction of the focal plane with data from (b). The working wavelength is 375 nm and the incident normal wave is in TM mode.

shown in Fig. 4(b), the focused spot is localized within the circle with the minimum curvature radius, indicating the presence of large transverse wavenumbers. As seen in Fig. 4(c), the spot size near the bottom planar surface of the hyperlens is about 15.6 nm (full-width at half-maximum (FWHM) corresponding to  $\lambda_0/24$ ), which is far less than the theoretically diffraction limited resolution of the single focusing lens ( $\approx 1.7\lambda_0$ ), and thus super-resolution focusing is realized. Figure 4 also shows that the beams are spreading when they leave away from the hyperlens. Therefore, the working plane should be as close to the bottom surface as possible in applications.

In optical data storage and other applications, the dimension of the incident beam is generally much larger than the value used in our simulation. However, as long as the numerical aperture of the focusing lens remains unchanged, the aperture and the focal length can be scaled in proportion to the actual size in order to meet the size of the beam in reality without disturbing the wavefront. Along with the unchanged mode of transmission, the device proposed is still applicable.

In conclusion, we report a new beam focusing device based on hyperlens to realize super-resolution beam

focusing. The device's working principle and characteristics such as resolution and transmission are discussed in detail. A multibeam focusing device is proposed, and numerical simulations have verified the effectiveness of the device. The simulated minimum beam spot size could be reduced to  $\lambda_0/24$ , which is far below the diffraction limit ( $1.7\lambda_0$ ). The newly proposed device, with its simple design structure, is expected to find numerous applications in the fields of optical data storage and nanophotolithography, among others.

This work was supported by the National Natural Science Foundation of China (No. 10904118), the Natural Science Foundation of Hubei Province (No. 2009CDB211), and the Fundamental Research Funds for the Central Universities.

## References

1. J. B. Pendry, *Phys. Rev. Lett.* **85**, 3966 (2000).
2. Ari Sihvola, *Metamaterials* **1**, 2 (2007).
3. J. B. Pendry, D. Schurig, and D. R. Smith, *Science* **312**, 1780 (2006).
4. D. R. Smith, S. Schultz, P. Markos, and C. M. Soukoulis, *Phys. Rev. B* **65**, 195104 (2002).
5. D. Schurig, J. B. Pendry, and D. R. Smith, *Opt. Express* **15**, 14772 (2007).
6. N. Fang, H. Lee, C. Sun, and X. Zhang, *Science* **308**, 534 (2005).
7. H. Qin, X. Li, and S. Shen, *Chin. Opt. Lett.* **6**, 149 (2008).
8. S. Durant, Z. Liu, J. M. Steele, and X. Zhang, *J. Opt. Soc. Am. B* **23**, 2383 (2006).
9. Z. Jacob, L. V. Alekseyev, and E. Narimanov, *Opt. Express* **14**, 8247 (2006).
10. Z. Liu, H. Lee, Y. Xiong, C. Sun, and X. Zhang, *Science* **315**, 1686 (2007).
11. Z. Jacob, L. V. Alekseyev, and E. Narimanov, *J. Opt. Soc. Am. A* **24**, 52 (2007).
12. J. Rho, Z. Ye, Y. Xiong, X. Yin, Z. Liu, H. Choi, G. Bartal, and X. Zhang, *Nat. Commun.* **1**, 143 (2010).
13. P. B. Johnson and R. W. Christy, *Phys. Rev. B* **6**, 4370 (1972).
14. W. Chen, M. D. Thoreson, S. Ishii, A. V. Kildishev, and V. M. Shalaev, *Opt. Express* **18**, 5124 (2010).
15. J. Li, D. Zhao, and Z. Liu, *Phys. Lett. A* **332**, 461 (2004).
16. C. P. Moore, R. J. Blaikie, and M. D. Arnold, *Opt. Express* **17**, 14260 (2009).